Arabian Journal of Chemistry (2020) **13**, 7045–7054

King Saud University

Arabian Journal of Chemistry

www.ksu.edu.sa
www.sciencedirect.com

ORIGINAL ARTICLE

Two Cu(II)-based coordination polymers: Photocatalytic dye degradation and treatment activity combined with BDNF modified bone marrow mesenchymal stem cells on craniocerebral trauma via increasing complement C3 expression

Jia-Peng Huang [a], **Ping Zhang** [b], **Jing-Gui Song** [c], **Jian Zhao** [d,*]

[a] *Basic Medical School, Heilongjiang University of Chinese Medicine, Harbin, Heilongjiang, China*
[b] *Department of Neurology, Henan Key Laboratory of Neurorestoration, the First Affiliated Hospital of Xinxiang Medical University, Xinxiang, Henan, China*
[c] *Department of Neurology, Henan Key Laboratory of Neurorestoration, the Second Affiliated Hospital of Xinxiang Medical University, Xinxiang, Henan, China*
[d] *Traditional Chinese Medicine Department, Second Affiliated Hospital of Heilongjiang University of Chinese Medicine, Harbin, Heilongjiang, China*

Received 1 May 2020; accepted 8 July 2020
Available online 15 July 2020

KEYWORDS

Coordination polym
Dye degradation;
X-ray sin diffra
tion;
BM

Abstract Two novel mixed-ligand Cu(II) coordination polymers (CPs) $\{[Cu_2(edpc)_2(ga)_2]\cdot 2H_2O\}_n$ (**1**) and $\{[Cu(edpc)(bpdc)]\cdot 0.25(H_2O)\}_n$ (**2**) (H_2ga = glutaric acid, edpc = 9-ethyl-2,6-di-pyridin-4-9*H*-carbazole, H_2bpdc = biphenyl-4,4′-dicarboxylic acid) have been solvothermally formed through a π-conjugated carbazole-containing pyridine ligand under the presence of auxiliary ligands (H_2ga for the complex **1** and H_2bpdc for complex **2**). Due to its good water stability of complex **2**, it was applied in the photocatalytic rhodamine B (RhB), methylene blue (MB) and methyl orange (MO) degradation in unclean water, and the possible pathway of photocatalytic degradation was researched. Whether the compounds could enhance the treatment activity of the BDNF modified bone marrow mesenchymal stem cells (BMSC) against craniocerebral trauma was then evaluated. The recognition of the craniocerebral trauma mice was assessed by Morris water maze (MWM). The viability of the nerve cells in the brain was evaluated by Cell Counting Kit-8 (CCK-8). Then the enzyme-linked immuno sorbent assay (ELISA) detection was performed to detect the release

* Corresponding author.
E-mail address: zhao_jian22@yeah.net (J. Zhao).
Peer review under responsibility of King Saud University.

Production and hosting by Elsevier

https://doi.org/10.1016/j.arabjc.2020.07.010

content of the brain-originated neurotrophic factor and nerve promoting factor β in peripheral regions of cerebral hemorrhage. Finally, the expression levels of the complement C3 receptor on the nerve cells in the brain was also determined.

1. Introduction

Craniocerebral trauma is a disease with a high lethality and disability, which brings a lot of burden to individual humans, families and even the whole society (Previgliano and Soto, 2019). For the treatment of craniocerebral trauma, people have been committed to the research about the removal of damaged brain tissue in order to reduce the primary and secondary injuries (Kulkarni et al., 2020). The usage of stem cells for the central nervous system injury treatment is a new strategy for the neural injury therapy that is widely concerned in the academic community at present, which brings a new dawn to the neurorepair treatment after craniocerebral injury (Erlangsen et al., 2020). Bone marrow mesenchymal stem cells (BMSC) can be broken up into neuronal cells in vivo, and secrete nerve promoting factors, brain-derived nerve promoting factors, etc. at the same time, and play a protective role in injured nerve tissue (Carballo-Cuello et al., 2020). Thus, in this present research, we aimed to explore the new candidates for the treatment of craniocerebral injury, and reveal the related mechanism at the same time.

In recent ten years, new functional coordination polymers (CPs) have attracted more and more attention in gas collection, catalysis, sensing field, magnetic pole, ion exchange and other industries (Lu et al., 2019; Li et al., 2016; Gu et al., 2019a, 2019b; Feng [illegible] al., 2019, 2017b). The final reactants are affected by various fact[illegible] as the types of metal ions and organic ligands, synthesis ope[illegible]on, operating temperature, solvent types, molar ratio and pH [illegible]ue (Feng et al., 2017a, 2013; Duan et al., 2020a, 2020b). In a word[illegible] reasonable coordination of organic ligands play[illegible]ortant [illegible] in the structure of target CPs. Based on pyridi[illegible]eriva[illegible]s, we ha[illegible] obtained a variety of CPs structures. Am[illegible]hem, V[illegible]e pyridin[illegible] ligands with rigid spacer group, because of the[illegible]bility, effectively decline the unexpecte[illegible]uatio[illegible]e synthesis. The ligands containing carbazole have[illegible]ng rigidity, [illegible]l conjugation, high fluorescence intensity, high[illegible] activity and [illegible] biological activity, so they are attracting [illegible]re an[illegible]e attention (Cheng et al., 2015, 2017; Yi et al., 2014[illegible]13). So the [illegible]s containing carbazole are regarded as an imp[illegible]t component for [illegible]rmation of CPs. At the same time, orga[illegible]olycar[illegible]ylic acid liga[illegible]ds have been largely used in the constr[illegible]n of [illegible]Ps due to their unique coordination method and high co[illegible] capabi[illegible] to metal ions.

In the p[illegible] study[illegible] new [illegible]ure Cu(II) coordination polymers (C[illegible]dpc)$_2$(g[illegible]}$_n$ (**1**) and {[Cu(edpc)(bpdc)]·0.25 (H_2O)[illegible]**2**) (H_2[illegible] = glutar[illegible]d, edpc = 9-ethyl-2,6-di-pyridin-4-yl-9[illegible]bazol[illegible] = biphenyl-4,4′-dicarboxylic acid) have been formed [illegible] π-co[illegible]ed carbazole-containing pyridine ligand under the[illegible]umstance of auxiliary ligands (H_2ga for the complex **1** and H_2bpdc [illegible]mplex **2**). Due to its good water stability of complex 2, it was applie[illegible] the photocatalytic rhodamine B (RhB), methylene blue (MB) and methyl orange (MO) degradation in unclean water, and the principle of photocatalytic degradation was researched. In biological experiment, the promotion activity of the compound on the brain derived neurotrophic factor (BDNF) modified bone marrow mesenchymal stem cells (BMSC) against craniocerebral trauma was assessed in vivo. The results of the Morris water maze (MWM) assay suggested that compound **1** has more powerful promotion ability than compound **2** on the increasing the BMSC treatment effect. The CCK-8 assay suggested that compound **1** could significantly increase the nerve cells viability. The ELISA detection further revealed that the release content of the brain-originated neurotrophic factor and nerve promoting factor β in peripheral regions of cerebral hemorrhage was obviously increased under compound **1** treatment instead of compound **2**. In the end, the western blot indicated, the enhancement activity of compound **1** was due to the up-re[illegible]ted expression of the complement C3 receptor on the nerve cel[illegible]n.

2. Experimental

2.1. Chemicals and mea[illegible]ments

All materials in t[illegible] exp[illegible] were [illegible]hased from the Beijing Bailingwe[illegible]agent co[illegible]ny a[illegible]sed in the experiment with no pu[illegible]on. Elemen[illegible]ysis of carbon, hydrogen and nitr[illegible] wa[illegible]rried out b[illegible] the PerkinElmer 240C analyzer. The Bruker [illegible]HA spectrometer was used to analyze the[illegible]amples obta[illegible] in the experiment, and the infrared [illegible]trum in the range o[illegible] 4000–400 cm^{-1} was recorded. The [illegible]mbda 950 [illegible]R-UV–vis spectrometer was used to analyze [illegible] diffuse re[illegible]tion spectroscopy (DRS) of the samples in th[illegible]avelen[illegible] range of 200–800 nm. The photocatalysis expe[illegible]s carried out using Bilon BL-GHX-V photo[illegible]hemical reactor. The processed materials were evaluated by [illegible]ADZU 2501PC UV–vis recording spectrophotometry.

2.2. Preparation and characterization for {[Cu_2(edpc)$_2$(ga)$_2$]·2H_2O}$_n$ (1) and {[Cu(edpc)(bpdc)]·0.25(H_2O)}$_n$ (2)

For the synthesis of complex **1**, 12 mg $Cu(NO_3)_2·6H_2O$ (0.05 mmol), 6.6 mg H_2ga (0.1 mmol), 8.7 mg edpc (0.05 mmol) and 5 mL of DMF/H_2O (ratio is 4:1) were mixed to form a solution. Next, the solution was poured into a 25.0 mL Parr Teflon-lined stainless steel vessel , then kept at 115 °C for 72 h. After cooling it to atmospheric temperature, wash the obtained blue shaped crystals and keep them dry. The final result was 45% percent, based on the weight of Cu. Anal. calcd for $C_{58}H_{54}N_6O_{10}Cu_2$: the carbon content is 61.82; the hydrogen content is 4.80; and the nitrogen content is 7.46 percent. Found (experimental): the carbon content is 61.85, the hydrogen content is 4.76 and the nitrogen content is 7.49 percent. IR (KBr, cm^{-1}): 3401(vs), 1607(vs), 1479(s), 1388(vs), 1294(m), 1228(s), 1162(s), 1133(w), 1071(w), 1036(w), 886(w), 807(s), 751(m), 682(w), 641(w), 608(w), 526(m).

For the synthesis of complex **2**, 12 mg $Cu(NO_3)_2·6H_2O$ (0.05 mmol), 12.1 mg H_2bpdc (0.05 mmol), 8.7 mg edpc (0.05 mmol) and 5 mL of DMF/H_2O (ratio is 4:1) were mixed to form a solution. Next, the solution was poured into a 15 mL Parr Teflon-lined stainless steel vessel, then kept at 100 °C for 72 h. After cooling it to atmospheric temperature, wash the obtained blue shaped crystals and keep them dry. The final result was 45% percent, based on the weight of Cu. Anal. calcd for $C_{38}H_{27.50}N_3O_{4.25}Cu$: the carbon content is 69.14; the hydrogen content is 4.10; and the nitrogen content is 6.37 percent. Found (experimental): the carbon content is 68.74, the

hydrogen content is 4.23and the nitrogen content is 6.26 percent. IR (KBr, cm^{-1}): 3409(s), 1678(s), 1610(vs), 1544(m), 1479(vs), 1381(vs), 1294(s), 1222(s), 1131(w), 1090(w), 1037 (m), 1011(s), 844(s), 808(s), 773(vs), 686(s), 606(m), 529(w), 438(m).

In order to obtain the data of X-ray, we use the Oxford Xcalibur E diffractometer. Statistical analysis of various strength data was performed using crysalispro software and the results were converted to HKL format. The pattern of SHELXS based on direct means was applied for establishing the initial structure models, and the pattern of SHELXL-2014 based on least square method was altered. The atom except hydrogen atom is refined by using different heterogenous parameters. Next, the whole of H atoms by using AFIX program to fasten on the C atom they are connected to. Table 1 shows the parameters and details of complex **1** and **2**.

2.3. Photocatalytic activity test

The photocatalytic activities of complexes **1** and **2** were evaluated by the photodegradation of RhB, MB and MO solutions at ambient temperature (298 K). The photocatalytic reactions were performed by a typical process: 25 mg of the coordination complex was dispersed in 100 mL aqueous solution of MB (6 mg L^{-1}), MO (6 mg L^{-1}) or RhB (6 mg L^{-1}) under a UV lamp, respectively. Before turning on the Hg lamp (400 W), the mixture was magnetically stirred in the dark for 30 min until an adsorption–desorption equilibrium was established at given intervals, and 5 mL of the reaction solution was periodically taken from the reactor and dispersed powders were removed by centrifugation. The separated samples were analyzed by UV–vis spectrophotometry. Degradation of the organic dyes under UV light irradiation without any complexes was also carried out for comparison.

Table 1 Refinement details and crystallographic parameters for complexes **1** and **2**.

Identification code	**1**	
Empirical formula	$C_{58}H_{54}Cu_2N_6O_{10}$	
Formula weight	1122.15	652
Temperature/K	296.15	293(2)
Crystal system	monoclin	monoclin
Space group	$P2_1/c$	C2/c
a/Å	18 (2)	2980(11)
b/Å	740(10)	8(2)
c/Å	0132(	8.1865(6)
α/°	0	90
β/°	(3)	98.9290(10)
γ/°	9	90
Volume/Å	526	3460.2(4)
Z	4	4
ρ_{calc}g/	415	1.252
μ/mm		0.673
Data/ restraints/para rs	9185/0/675	3049/70/215
Goodness-of-fit F^2	1.014	1.088
Final R indexes [I ≥ 2σ (I)]	R_1 = 0.0403, ωR_2 = 0.1112	R_1 = 0.0673, ωR_2 = 0.1947
Final R indexes [all data]	R_1 = 0.0493, ωR_2 = 0.1151	R_1 = 0.0768, ωR_2 = 0.2024
Largest diff. peak/hole/e Å^{-3}	0.77/−0.85	0.70/−0.61
CCDC	1,999,757	1,999,768

2.4. Morris water maze (MWM)

After the synthesis of compounds **1** and **2** in this present research, their enhancement activity against craniocerebral trauma after planted with BDNF m ne marrow mesenchymal stem cells were evalu by de ining the cognitive function in mice. Thus, t orris wate ze measurement was operated in the s dy u the inst ions. In short, the 50 mice used in ne study e ob ned from the Zhejiang university ngzho Chin then kept at the standard enviro nt wi ample wat r and aliment. All the operation i the was ad ed by the Ethics Committee of t Zhejian iversi (Hangzhou, China). Intracerebral rrhage mod made by injecting heparin and c gen sing brain reotactic method. Three days later, GDNF/B Cs were transplanted into brain combined ompound 2 for treatment at the concentratio 5 mg/kg for 12 h. The MWM was conducted and the ti of the m finished the MWM was recorded and an zed.

2.5. Ce g Kit-8 (CCK-8)

the viability of the nerve cells in the brain during raniocerebral trauma, the Cell Counting Kit-8 was operated in the study after compound **1** or **2** treatment with GDNF/BMSCs transplantation. All the preformation was finished according to the protocols. In short, the growing neurons in the logical growth were collected and seeded into 96 well plates at the concentration of 10^4 cells per well. The neurons were first cultured at 37 °C and 5% CO_2 for 12 h, then incubated with compounds **1** and **2** (1, 2, 4, 8, 10, 20, 40, 80 μg/mL) for 48 h. Next, the cell medium was removed and replaced with new medium with 10% CCK-8 reagent. Finally, the absorbance of each wells was measured and analyzed from three repeats.

2.6. ELISA detection

After compound **1** or **2** treatment, the content of the brain-originated neurotrophic factor and nerve promoting factor β released into peripheral regions of cerebral hemorrhage was evaluated by ELISA detection kit. This measurement was conducted in accordance with the instruments with a little modification. Briefly, the brain stereotactic method was used to establish the hemorrhage model, then the GDNF/BMSCs were transplanted into brain combined with compound **1** or **2** for treatment at the concentration of 5 mg/kg for 12 h. Subsequently, the cerebrospinal fluid of the nice in different groups was collected and the quantity of growth factors was evaluated. This study was conducted three times and the results were showed as mean ± SD.

2.7. Western blot

The western blot was carried out to evaluate the expression ability of the complement C3 receptor on the nerve cells differentiated from GDNF/BMSCs in the brain. All preformation was under the manufactures' protocols. Briefly, the brain stereotactic method was used to establish the hemorrhage model, then the GDNF/BMSCs were transplanted into brain combined with compound 1 or 2 for treatment at the concentration of 5 mg/kg for 12 h. The nerve cells in the brain were collected and the total protein was extracted. The BCA detection kit was used to evaluate the protein concentration. Next, all the samples were loaded on SDS-PAGE gel and electrophoretically transformed to a 0.22 mm (PVDF) membrane. After blocked with 5% nonfat milk for 2 h, the primary antibody and secondary antibody conjugated with horseradish peroxidase was used to incubate the PVDF membrane. Chemi-Doc™ Touch Imaging System (Bio-Rad, Hercules, California, USA) was used to capture the images.

3. Results and discussion

3.1. Molecular structure

According to the results of single crystal X-ray diffraction, complex **1** crystallized in monoclinic $P2_1/c$ space group. The asymmetric part of **1** is composed of two mutually independent Cu(II) cations, double edpc ligands and two different ga^{2-} anions. Fig. 1a shows that the coordination structures of Cu (1) and Cu(2) are different. Cu(1) atom is composed of two O atoms from different ga^{2-} and two N atoms from different edpc ligands to form a five coordinated form, which is a twisted triangular biconical structure[CuN_2O_3]. Cu(2) atom is surrounded by four O atoms of two kinds of ga^{2-} and two N atoms from different edpc ligands. It has a deformed [CuN_2O_4] octahedral geometry. The length of Cu-N bond is 1.980(2) to 2.074(2) Å and the length of Cu-O bond is 1.902(2) to 1.953 (3) Å, all of which are normal. There are two different coordination modes of ga^{2-} anions in **1**. Fig. [illegible]s that deproton carboxyl group of the H_2ga ligand c[illegible]dinate[illegible]h Cu(1) is in the mode of μ_1-η^1:η^1, and the H_2[illegible]and coord[illegible]ed with Cu (2) is in the mode of μ_1-η^1:η^1 and μ_1[illegible]^0. As sho[illegible]in Fig. 1c, the edpc ligand bridges th[illegible]d(II) ca[illegible]s to t[illegible]eft-handed helix chain L1 along th[illegible]axis by two[illegible]e arms in the form of μ_2 bridging [illegible]rdinat[illegible], while t[illegible] carboxyl group from ga^{2-} bridges the [illegible]U[illegible]ations t[illegible]the left-handed helix chain L2 along[illegible] c-axis [illegible]cordin[illegible] Fig. 1d, the adjacent helical chain[illegible]m a two-di[illegible]al structure based on the same Cu[illegible] c[illegible]s interco[illegible]tion. Through topological analysis, this stru[illegible] can be clearly shown. Taking Cu(II) as a[illegible]nection no[illegible]ga^{2-} and edpc anion as junctions, **1** c[illegible]e seen as a 4-conne[illegible]ion **sql** network with the dot symbol [illegible]$\cdot6^2$}. The lattice water molecule O10 forms a strong hydro-[illegible] bond betw[illegible]n the (4,4) network layer and the coordination c[illegible]xylic ox[illegible]n atoms O4, O5. The Cu(1) cation bridge is

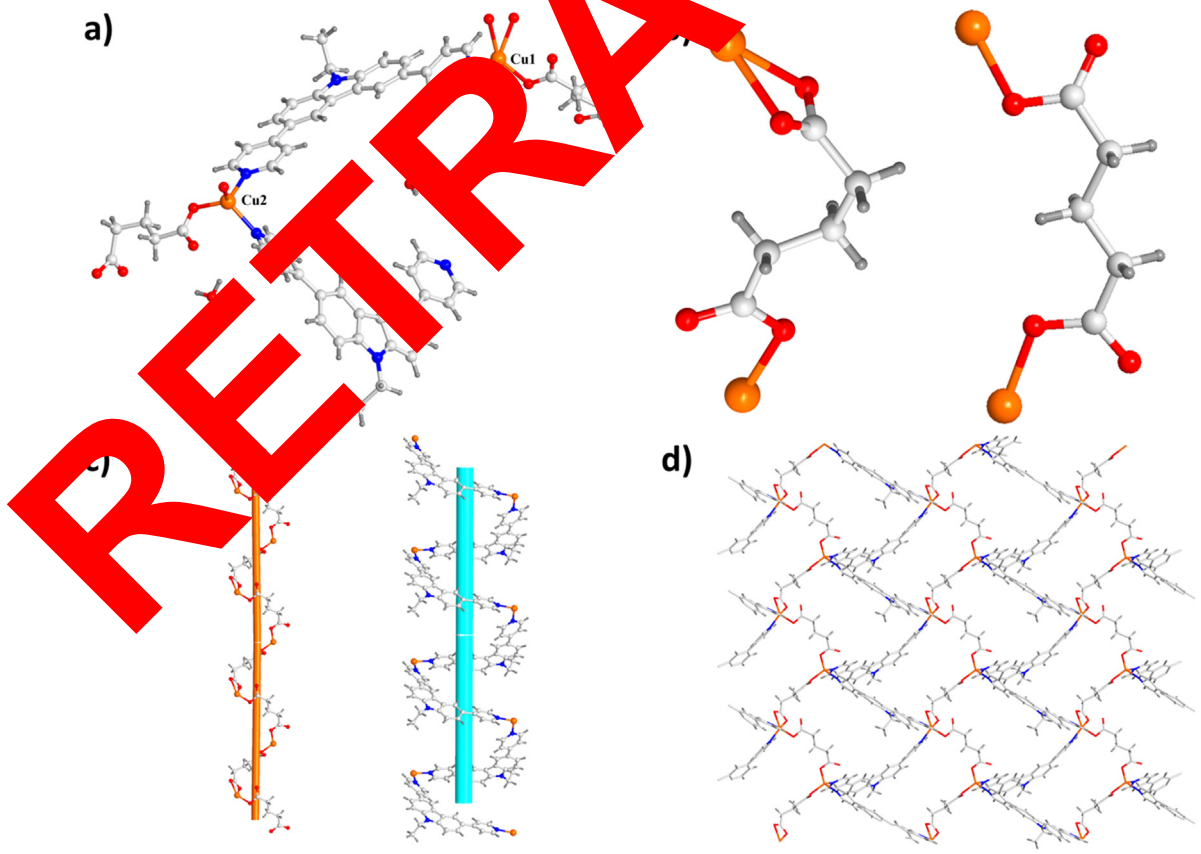

Fig. 1 (a) Image for the asymmetry part of **1**. (b) The coordination modes for the ga^{2-} ligands. (c) The helical chains found by link of the ligands with the Cu(II) ions. (d) The 2D layered framework of **1**.

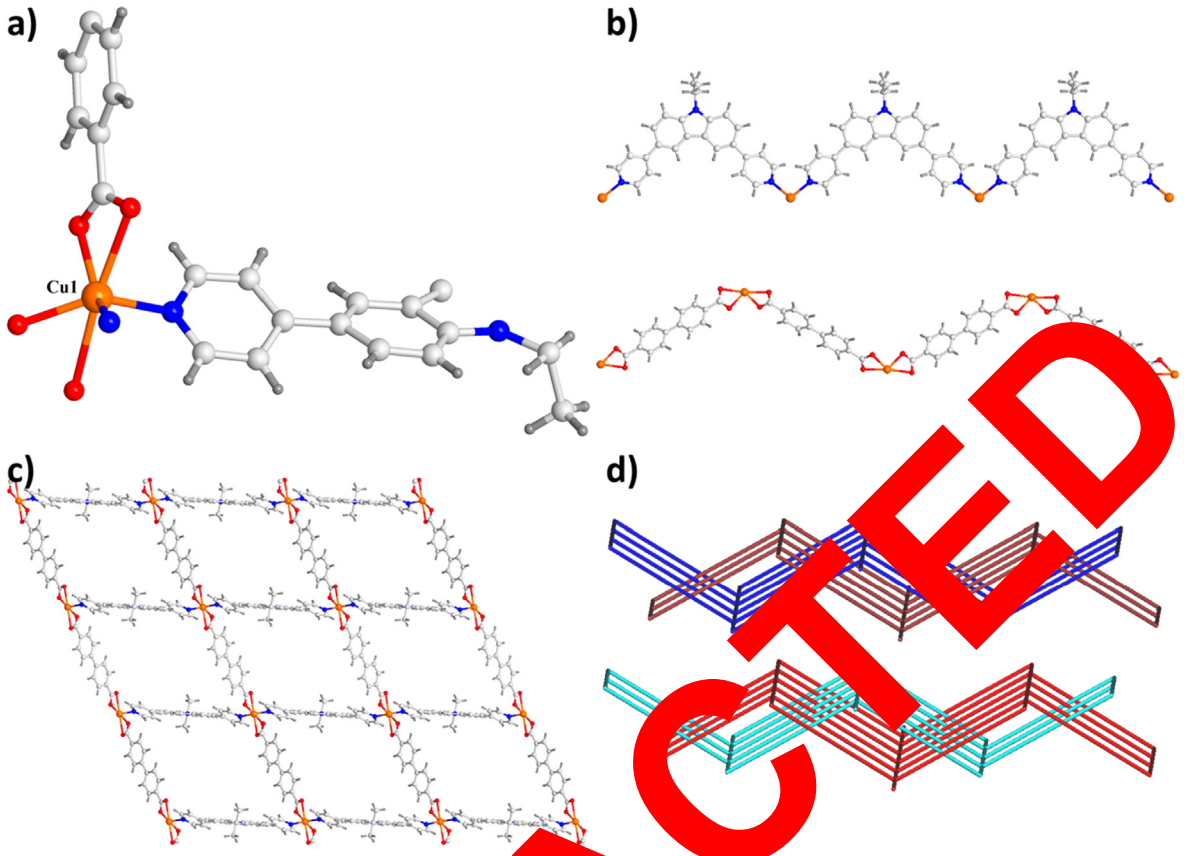

Fig. 2 (a) Image for asymmetric part of complex **2**. The 1-d[illegible]ins found by the link of the ligands with Cu(II) ions. (c) The two-dimension layered framework of **2**. (d) The 2-fold interpe[illegible]ated [illegible]rk of complex **2**.

connected to the right-hand helical chain R[illegible]g the [illegible]xis. In addition, the adjacent two-dimensional f[illegible]work [illegible]nged in ···AAAA··· parallel is connected int[illegible] tw[illegible] ered structure through the hydroge[illegible]ond.

According to the results of si[illegible]rystal X-ra[illegible]ffraction, complex 2 belongs to the m[illegible]chi[illegible]2/*c* space g[illegible]up. The asymmetric part of **2** con[illegible]ts of a sin[illegible]Cu(II) ion, a single edpc ligand, a single b[illegible]− ligand and [illegible]quarter of water molecule. Fig. 2a sho[illegible]that C[illegible]1) is hexahe[illegible]ral in octahedral coordination envi[illegible]ent, [illegible]ch is formed by four O atoms from two chelated [illegible]e carbo[illegible]ic acid groups in two $bpdc^{2-}$ ligan[illegible]d two [illegible]toms [illegible]m different edpc ligands. As show[illegible] Fig[illegible]b, edpc[illegible]s connect Cu(II) cations to shape[illegible]infinite[illegible]ne-dimens[illegible]nal linear chain. The distance betwee[illegible]a[illegible]2980 Å, and the angle of Cu-Cu-Cu is 180.[illegible]Next, through the coordination of the carboxyl group of b[illegible]− with Cu(II) cation, another infinite one-dimensional *zig*[illegible]chain with Cu-Cu distance of 15.1678 Å and Cu-Cu-Cu angle of 124.475° is formed. In the end, the two chains are connected in a highly undulating two-dimension framework. In this structure, every 6-membered ring is shaped by 4 Cu(II) cations, 2 edpc and 2 $bpdc^{2-}$ ligands, with a size of 25.2943 × 16.9816 Å (diagonal length). From the topological point of view, Cu(II) cation can be regarded as 4-connected nodes, and edpc and $bpdc^{2-}$ ligands can be regarded as connecters; therefore, two-dimension network can be written as a stacked $4^4{\cdot}6^2$-**sql** framework, including a window of 15.298 × 14.805 Å (Fig. 2c). The high fluctuation of such a large network window and a **sql** table admits two adjacent tables to infiltrate each other in a parallel pattern, thus forming a 2D framework (Fig. 2d).

3.2. Photocatalytic activities

Fig. 3 shows the UV/Vis reflection spectra of **1** and **2**. According to the graph drawn by Kubelka-Munk method $(F(R)\,hm)^{0.5}$, band gap energy E_g was defined by the intersection of the energy axis and the line extrapolated from the linear part of the absorption edge, where h represents the Planck constant, M represents the frequency of electromagnetic wave, and R represents the reflectivity of infinite thick layer at a certain wavelength. As for the Kubelka-Munk method, $F(R) = (1 - R)^2/2R$ was transformed from the logged diffuse reflection data. As shown in Fig. 3, the E_g estimate of **1** is 3.28 eV, and that of 2 is 2.71 eV. It is suggested that complexes **1** and **2** may respond to UV light and have potential photocatalytic activity. Considering the following dye degradation experiments, it is essential to research their water stability. Complexes **1** and **2** were soaked in water and the results show that complex **1** quickly decomposes while complex **2** could keep its crystallinity.

The catalytic properties of complex **2** were studied by measuring the effects of complex **2** on rhodamine B (RhB), methylene blue (MB) and methyl orange (MO), which are common organic dyes in the industrial wastewater (Banasz and Wałęsa-Chorab, 2019; Yuan et al., 2020; Ren et al., 2017;

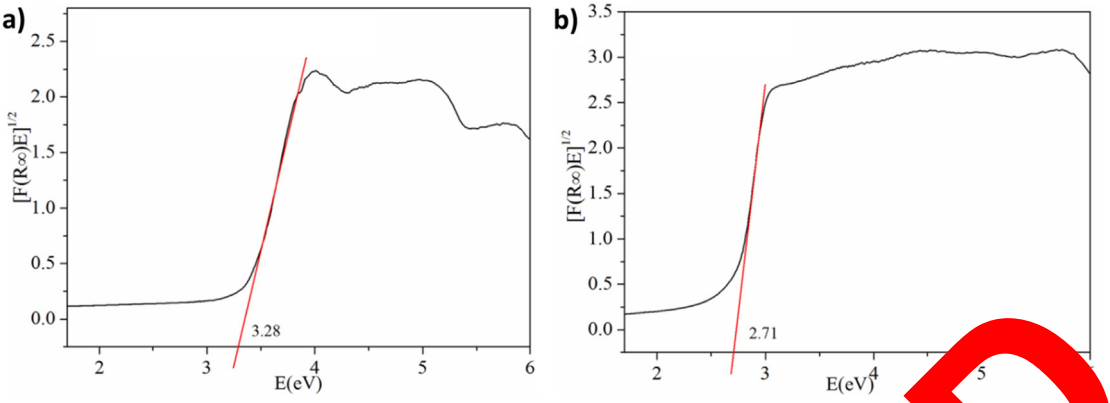

Fig. 3 the UV/V reflection spectra and energy (eV) of **1** (a) and **2** (b).

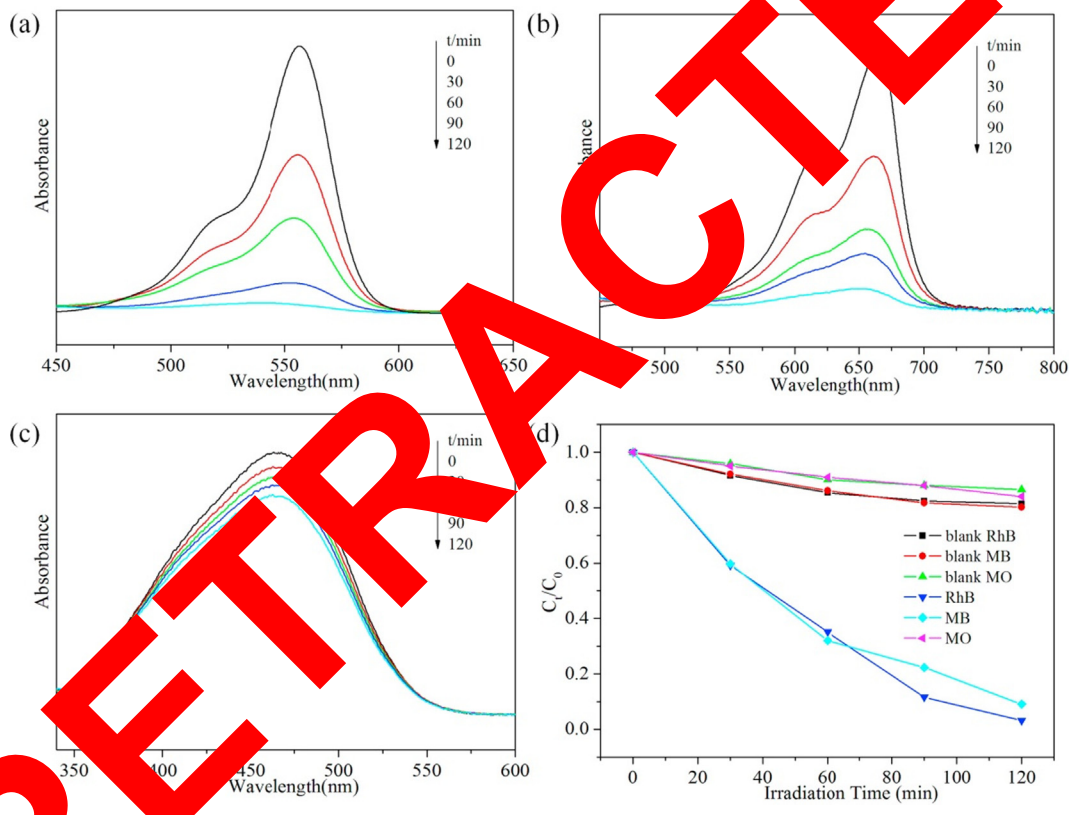

Fig. Absor[illegible]ctra of (a) RhB, (b) MB and (c) MO solution during the degradation reaction by using **2**; (d) plots of concentration ratios [illegible]O C_t/C_0 against irradiation time (min) under the circumstance of **2** during the degradation reaction under UV irradiation

Patroniak et al., 2006; Marcinkowski et al., 2017, 2015; Wei et al., 2020; Jawad et al., 2019, 2016, 2015; Jawad, 2019). It should be noted that as a kind of photocatalyst, **2** is insoluble in water. Therefore, the experimental conditions were 165 W mercury lamp ultraviolet light irradiation, and the photocatalytic activity of **2** was assessed by reacting with these dye solutions. We monitored the decomposition of RHB, MB and MO at 464 nm, 54 nm and 664 nm. At the same time, we gave the time-resolved absorption spectra of **2** for three substances. Fig. 4a shows the degradation of RhB solution by **2**. According to the figure, the maximum absorbance of the solution at 554 nm decreased gradually with the increase of illumination time. Moreover, the decomposition rate of RhB was 97% after two hours of UV irradiation and half an hour of standing. Fig. 4b shows the degradation of MB by **2**. The decomposition rate of MB was 91% after two hours of UV irradiation. In the same environment, the photocatalytic degradation of MO by complex **2** is weak (Fig. 4c). Fig. 4d shows that under UV irra-

diation, the decomposition rate of MB, RhB and Mo at the circumstance or absence of **2**. So the complex is very good at photocatalytic degradation of RhB and MB. To detect this selective effect, we compared the structures of MB, MO and RhB. It could be found that MO has azo groups, but RhB and MB have different structures. For complex **2**, the selective degradation of RhB and MB may depend on whether the structure of the pollutant contains azo group.

Based on the literature review and the above experiments, the following conclusions about the photocatalytic mechanism of degradation are obtained (Jawad et al., 2019, 2016, 2015; Jawad, 2019). In the UV environment, the electrons (e^-) in the highest polymer orbit are excited and transferred to the lowest unoccupied molecular orbit, leaving holes (h+) in Homo. The e− and h+ transfer to the surface of catalyst, and oxygen molecules (O_2) are transformed to oxygen radicals ($\cdot O_2^-$) by electrons, and finally converted to hydroxyl radicals (·OH). At the same time, h+ oxidize H_2O to hydroxyl radicals (·OH). These ·OH have the ability to disintegrate organic dyes efficiently.

3.3. Compound shortened the time spent by the mice in finishing MWM assay

Compounds **1** and **2** were synthesized for the evaluation of the enhancement activity against craniocerebral trauma after planted with GDNF/BMSCs. Thus, the MWM assay was performed in this experiment to detect the time spent by the mice finishing this experiment. Fig. 5 indicates that after transplantation of the GDNF/BMSCs in the mice brain, the time spent by the mice in finishing MWM assay was slightly shortened. On the 7th day, the normal animal spent about 5 min during the finishing MWM assay, while the model mice spent about 17 min, which is significantly higher than the control group. However, in combination with compound **1**, the time was obviously reduced to 6 min and 14 min, which is significantly differs from the GDNF/BMSCs group. While, compound **2** showed almost no enhancement activity on the time shorting.

3.4. Compound increased the viability of the nerve cells

As we have proved in the above results, compound **1** displayed more powerful protective activity on the hemorrhage model than compound **2**. So, in the study, the effect of the compounds on the activity of the nerve cells was also determined. Fig. 6 indicated that the during damaging procession compound **1** treatment could obviously raise the survival rate of the nerve cells, while compound **2** conducted no influence on the cell activity. This result was consistence with the previous results showed in Fig. 6.

3.5. Compound increased the content of brain-derived neurotrophic factor and nerve growth factor β in peripheral regions of cerebral hemorrhage

As the nerve cells differentiated from GDNF/BMSCs in the brain could produce the nerve growth factor β in peripheral regions of cerebral hemorrhage, which is vital important for the nerve cells survival and growth, in this research, the ELISA detection was used for concentration measurement of the growth factor in the peripheral regions of cerebral hemorrhage. The data in Fig. 7 indicated that in the model group, the was less growth factors than other groups. While, after compound **1** treatment combined with GDNF/BMSCs transplantation, the releasing levels of the growth factors were significantly increased, but the biological function of compound was not observed (see Fig. 8).

3.6. Compound stimulated the expression level of the complement C3 receptor on the nerve cells differentiated from GDNF/BMSCs

The complement C3 receptor on the nerve cells could not only regulate the secretion of the brain-original neurotrophic factor and nerve promoting factor β into peripheral regions of cerebral hemorrhage, but also influence the survival and growth of the nerve cells. So the western blot in this this research

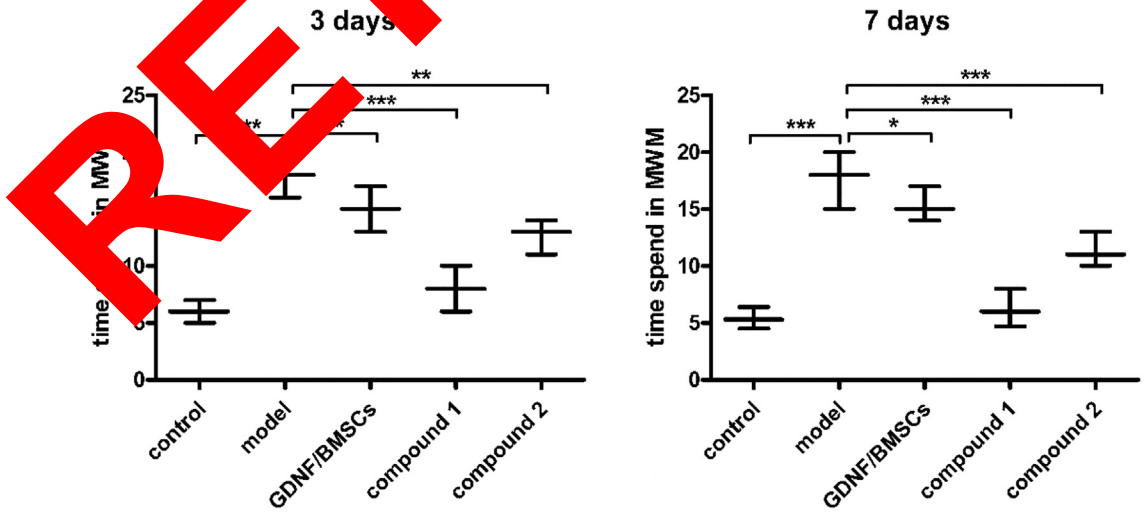

Fig. 5 Shortened time spent by the mice in finishing MWM assay under compound treatment after GDNF/BMSCs transplantation. The brain stereotactic method was used to establish the hemorrhage model, then the GDNF/BMSCs were transplanted into brain combined with compound **1** or **2** for treatment. The MWM assay was conducted to evaluate the cognitive function of the mice.

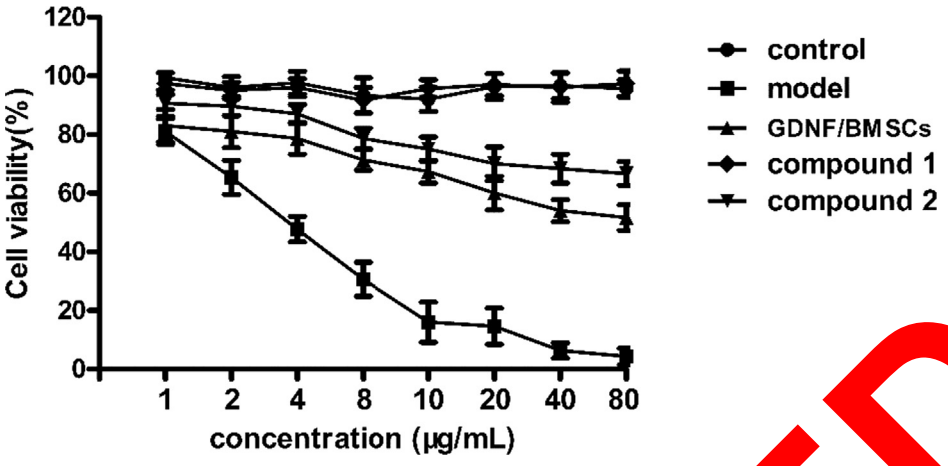

Fig. 6 Increased viability of the nerve cells after compound exposure. The nerve cells were pl[illegible]d into [illegible] well p[illegible]nd undergo the hypoxia treatment, then compound **1** or **2** was used for treatment. The CCK-8 was conduct[illegible]r the[illegible]ve cell assessment.

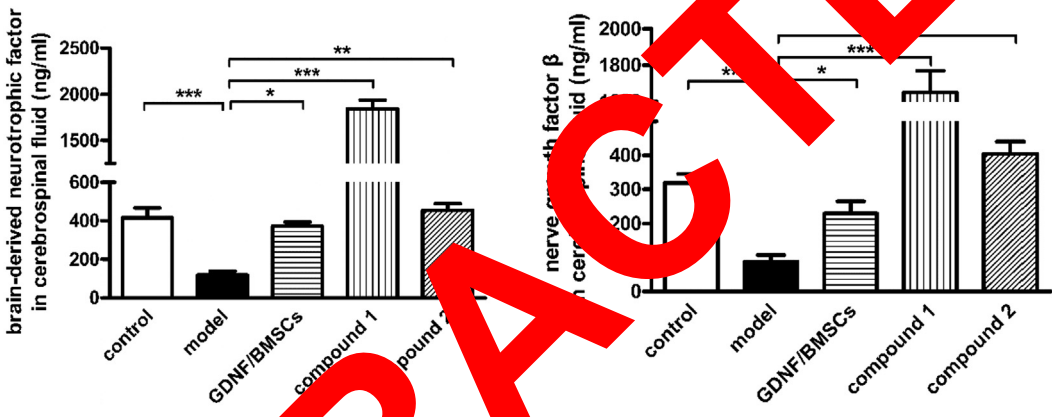

Fig. 7 Increased content of brain-orig[illegible] neu[illegible]factor and nerve promoting factor β in peripheral regions of cerebral hemorrhage. The brain stereotactic p[illegible]od [illegible]d to estab[illegible]n the hemorrhage model, then the GDNF/BMSCs were transplanted into brain combined with compound **1** [illegible] for treati[illegible]. The growth factors in peripheral regions of cerebral hemorrhage were evaluated with ELISA detection kit.

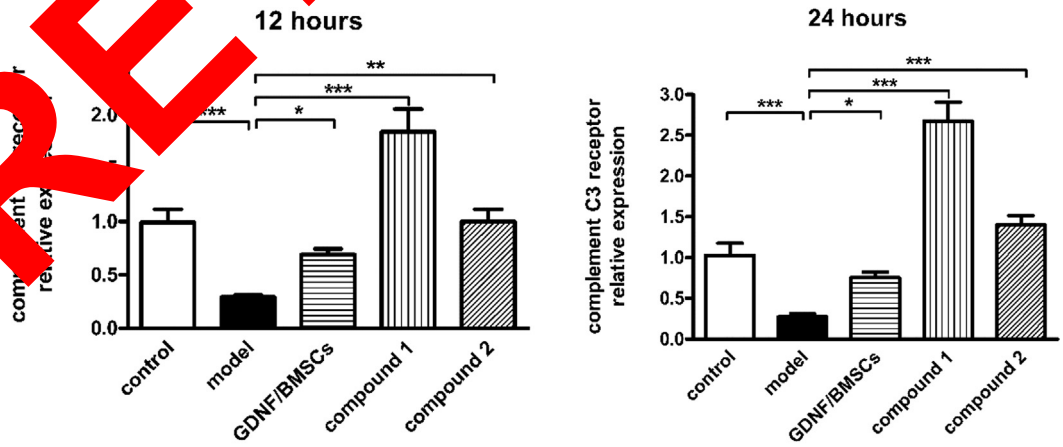

Fig. 8 Stimulated expression level of the complement C3 receptor on the nerve cells differentiated from GDNF/BMSCs under compounds treatment. The brain stereotactic method was used to establish the hemorrhage model, then the GDNF/BMSCs were transplanted into brain combined with compound **1** or **2** for indicated treatment. Western blot conducted in the study was used for complement C3 receptor expression measurement.

was used to determine the complement C3 receptor expression level on the cells. Compared with the model group or the GDNF/BMSCs group, compound **1** could further increasing the up-regulated level of complement C3 receptor on the nerve cells. Total different from compound **1**, compound **2** has no incentive function on the C3 receptor expression.

4. Conclusion

In conclude, we have smoothly formed two fresh mixed Cu(II) coordination polymers (CPs) through a π-conjugated carbazole-containing pyridine ligand under the circumstance of auxiliary ligands (H_2ga for complex **1** and H_2bpdc for complex **2**). The single crystal X-ray diffraction research shows that complex **1** shows a 2D layered framework based on the helical chains and complex **2** demonstrates a 2-fold interpenetrated network. Due to its good water stability of complex **2**, it was applied in the photocatalytic rhodamine B (RhB), methylene blue (MB) and methyl orange (MO) degradation in unclean water, and the principle of photocatalytic degradation was researched. In addition, serious experiments were performed to detect the promotion activity of the compound on the BDNF modified bone marrow mesenchymal stem cells (BMSC) against craniocerebral trauma. We found that compound **1** has more powerful incentive function than compound **2** on the increasing the BMSC treatment effect, which is confirmed by the Morris water maze (MWM) assay. The CCK-8 assay pointed out that compound **1** could significantly increase the nerve cells viability. The ELISA detection further revealed that the release content of the brain-original neurotrophic factor and nerve promoting factor β in peripheral regions of cerebral hemorrhage was obviously increased under compound **1** treatment instead of compound **2**. In the end, the western blot pointed out that the enhancement activity of compound **1** was sue to the up-regulated expression of the complement C3 r tor on the nerve cells in the brain. In conclusion, compare with c pound **2**, compound **1** is more talent on the promotion activity BDNF modified bone marrow mesenchymal stem ells (BMSC against craniocerebral trauma.

5. Data availability

The data used to support the findi of this stud e included within the article.

Declaration of Competi terest

The authors de e that y have no known competing financial interests o l relati ships that could have appeared to i fluence t ork re ted in this paper.

Ackno gments

The resea as supported by Youth Development Fund project of the t Affiliated Hospital of Xinxiang Medical University (Q 19-A04) and Henan Key Laboratory of Neurorestoratology (HNSJXF-2018-007).

References

Banasz, R., Wałęsa-Chorab, M., 2019. Polymeric complexes of transition metal ions as electrochromic materials: synthesis and properties. Coord. Chem. Rev. 389, 1–18.

Carballo-Cuello, C., de Jesus, O., Fernandez-de Thomas, R.J., Garcia, M., Vigo-Prieto, J., de Jesus-Espinosa, A., 2020. Posttraumatic hydrocephalus in pediatric patients after decompressive craniectomy. World Neurosurg. 136, e690–e694.

Chen, D.H., Lin, L., Sheng, T.L., Wen, Y.H., Hu, S.M., Fu, R.B., Zhuo, C., Li, H.R., Wu, X.T., 2017. Syntheses, structures and luminescence properties of five coordination polymers based on designed 2,7-bis(4-benzoic acid)-N-(4-benzoic acid) carbazole. CrystEngComm 19, 2632–2643.

Cheng, H.J., Tang, H.X., Shen, Y.L., Xia, N.N., Yin, W.Y., Zhu, W., Tang, X.Y., Ma, Y.S., Yuan, R.X., 2015. Carboxylate ligands induced structural diversity of zinc(II) coordination polymers based on 3,6-bis(imidazol-1-yl)carbazole: syntheses, structures and photocatalytic properties. J. Solid State Chem. 232, 200–206.

Duan, C., Yu, Y., Yang, P., Zhang, X., Li, F., Li, L., Xi, H., 2020a. Engineering new defects in MIL-100(Fe) via a mixed-ligand approach to effect enhanced volatile organi und adsorption capacity. Ind. Eng. Chem. Res. 59, 774 .

Duan, C., Yu, Y., Xiao, J., Zhang, X., L Yang, P., J., Xi, H., 2020b. Water-based routes for synt of metal-or c frameworks: a review. Sci. China M . 63, 685.

Erlangsen, A., Stenager, E., Co , Y., Ande P.K awton, K., Benros, M.E., Nordente M., St ger, L . Association between neurological ders a eath by su ide in Denmark. JAMA 323, 444–45

Feng, X., Ling, X.L d, L., W L.Y., N .W., Su, B.Y., 2013. A series of 3D anide fram k nstructed from aromatic multi-carb and: Structu iversity, luminescence and magnetic p opertie lton T. 42, 10292–10303.

Feng, X., Feng, Y.Q., Gu Sun, Y.L., Zhang, T., Ma, L.F., Wang, L a. Series d–f onuclear metal–organic frameworks: or tunability and luminescent probe with switchable properties. org. Chem. 1713–1721.

Fe X., Guo, N hen, H.P., Wang, H.L., Yue, L.Y., Chen, X., Ng, Liu, X Ma, L.F., Wang, L.Y., 2017b. A series of anionic ho on polymers, based on azoxybenzene carboxylate: structures, luminescence and magnetic properties. Dalton T. 46, 92–14200.

g Shang, Y., Zhang, H., Li, R., Wang, W., Zhang, D., Wang, L., Li, Z., 2019. Enhance luminescence and tuning magnetic properties of lanthanide coordination polymers based on fluorine substituted and phenanthroline ligands. RSC Adv. 9, 16328–16338.

Gu, J., Wen, M., Cai, Y., Shi, Z., Arol, A.S., Kirillova, M.V., Kirillov, A.M., 2019a. Metal-organic architectures assembled from multifunctional polycarboxylates: hydrothermal self-assembly, structures, and catalytic activity in alkane oxidation. Inorg. Chem. 58, 2403–2412.

Gu, J., Wen, M., Cai, Y., Shi, Z., Nesterov, D.S., Kirillova, M.V., Kirillov, A.M., 2019b. Cobalt(II) coordination polymers assembled from unexplored pyridine-carboxylic acids: structural diversity and catalytic oxidation of alcohols. Inorg. Chem. 58, 5875–5885.

Jawad, A.H., 2019. Adsorption and mechanism study for methyl orange dye by cross-linked chitosan-ethylene glycol diglycidyl ether beads. Desalin. Water Treat. 166, 377–386.

Jawad, A.H., Alkarkhi, A.F.M., Mubarak, N.S.A., 2015. Photocatalytic decolorization of methylene blue by an immobilized TiO_2 film under visible light irradiation: optimization using response surface methodology (RSM). Desalin. Water Treat. 56, 161–172.

Jawad, A.H., Mubarak, N.S.A., Ishak, M.A.M., Ismail, K., Nawawi, W.I., 2016. Kinetics of photocatalytic decolourization of cationic dye using porous TiO_2 film. J. Taibah Univ. Sci. 10, 352–362.

Jawad, A.H., Razuan, R., Appaturi, J.N., Wilson, L.D., 2019. Adsorption and mechanism study for methylene blue dye removal with carbonized watermelon (Citrullus lanatus) rind prepared via one-step liquid phase H_2SO_4 activation. Surf. Interfaces 16 (2019), 76–84.

Kulkarni, C., Mohite, S., Meshram, V., 2020. Unplanned complex suicide by self-stabbing and rail suicide: a case report and review of literature. Am. J. Forensic. Med. Pathol. 41, 78–80.

Li, Y., Xu, H., Ouyang, S., Ye, J., 2016. Metal–organic frameworks for photocatalysis. Phys. Chem. Chem. Phys. 18, 7563–7572.

Lu, J., Feng, J., Ma, X., Wang, P., Xu, B., He, P., Jia, J., Ma, P., Niu, J., Wang, J., 2019. A new phosphotungstate-supported rhenium carbonyl derivative: synthesis, characterization and catalytic selective oxidation of thiophenes. CrystEngComm 21, 7322–7328.

Marcinkowski, D., Wałęsa-Chorab, M., Kubicki, M., Hoffmann, M., Kądziołka, G., Michalkiewicz, B., Patroniak, V., 2015. A new 2,6-di(anthracen-9-yl)pyridine ligand and its complexes with Ag(I) ions: synthesis, structure and photocatalytic activity. Polyhedron 90, 91–98.

Marcinkowski, D., Wałęsa-Chorab, M., Bocian, A., Mikołajczyk, J., Kubicki, M., Hnatejko, Z., Patroniak, V., 2017. The spectroscopic studies of new polymeric complexes of silver(I) and original mononuclear complexes of lanthanides(III) with benzimidazole-based hydrazine. Polyhedron 123, 243–251.

Patroniak, V., Lehn, J.M., Kubicki, M., Ciesielski, A., Wałęsa, M., 2006. Chameleonic ligand in self-assembly and synthesis of polymeric manganese(II), and grid-type copper(I) and silver(I) complexes. Polyhedron 25, 2643–2649.

Previgliano, I., Soto, M.A., 2019. A case report on the use of pharmacological intervention in the treatment of diffuse axonal injury from road traffic accidents. J. Med. Life 12, 468–470.

Ren, Y.N., Xu, W., Zhou, L.X., Zheng, Y.Q., 2017. Efficient tetracycline adsorption and photocatalytic degradation of rhodamine B by uranyl coordination polymer. J. Solid State Chem. 251, 105–112.

Wei, X.J., Hao, Z.C., Han, C., Cui, G.H., 2020. Syntheses, crystal structures and photocatalytic properties of three zinc (II) coordination polymers constructed by mixed ligands. J. Mol. Struct. 1200, 127117.

Yi, X.C., Xi, F.G., Wang, K., Su, Z., Gao, E.Q., 2013. Synthesis, structure and properties of zinc(II) coordination polymers with 9H-carbazole-2,7-dicarboxylic acid. J. Solid State Chem. 206, 293–299.

Yi, X.C., Huang, M.X., Qi, Y., Gao, E.Q., 2014. Synthesis, structure, luminescence and catalytic properties of [illegible]m(ii) coordination polymers with 9H-carbazole-2,7-dica[illegible]ylic [illegible] Dalton T. 43, 3691–3697.

Yuan, F., Yu, H.S., Yuan, C.M., Zho[illegible]G., Li, F., Lu[illegible]J., Ling, X. Y., Wang, J., Singh, A.[illegible]umar,[illegible] 2020. [illegible]ctures and photocatalytic properties [illegible]wo Mn(II)[illegible]d c[illegible]nation polymers. Inorg. Chim. Ac[illegible]99, 119[illegible]9.